Understanding the origin of high corrosion inhibition efficiency of bee products towards aluminium alloys in alkaline environments

Jacek Ryl[#,1], Joanna Wysocka[1], Mateusz Cieslik[1], Husnu Gerengi[3], Tadeusz Ossowski[2], Stefan Krakowiak[1] and Pawel Niedzialkowski[2]

[1] Department of Electrochemistry, Corrosion and Materials Engineering, Faculty of Chemistry, Gdansk University of Technology, Narutowicza 11/12, 80-233 Gdansk, Poland

[2] Department of Analytical Chemistry, Faculty of Chemistry, University of Gdansk, Wita Stwosza 63, 80-308 Gdansk, Poland

[3] Corrosion Research Laboratory, Department of Mechanical Engineering, Faculty of Engineering, Duzce University, 81620, Duzce, Turkey

[#] Corresponding author: jacek.ryl@pg.edu.pl

Abstract

Various bee products were found to be efficient corrosion inhibitors of aluminium in different environments. In particular, bee pollen was found to be highly effective in alkaline electrolytes, yet its highly complex composition and possible synergistic interactions hinder determination of the compounds acting as active corrosion inhibitors. The main purpose of the following work is to investigate the effect of solvents used for pollen extraction process on the corrosion inhibition of AA5754 alloy in alkaline environment. Both infrared and mass spectroscopies as well as chromatographic analysis were used to determine differences in the composition of each obtained extract.

The inhibition efficiency ($IE_\%$) of each extract was determined by using the potentiodynamic polarization and impedance studies. The highest $IE_\%$, exceeding 90% at 10 gL^{-1}, was recorded for the water/ethanol extract. Most importantly, it has been found that the dichloromethane extract containing less polar compounds enhanced the corrosion rate at low bee pollen concentrations, and offered lower inhibition efficiency at the concentrations above 10 gL^{-1}. The adsorption isotherms were drawn based on dynamic impedance spectroscopy in galvanostatic mode (g-DEIS), while the measurements carried out at elevated temperatures allowed the construction of Arrhenius plots and, consequently, the confirmation of the physical mechanism of adsorption.

1.   Introduction

The application of corrosion inhibitors is one of the most widely used methods for preventing the accelerated degradation of aluminium and its alloys under aggressive corrosion conditions. Synthetic chemical compounds that efficiently inhibit corrosion, are often toxic and expensive. Because of increasing ecological awareness and stricter regulations on the environmental protection in relation to the usage and utilization of man-made corrosion inhibitors, the search for environment-friendly alternatives, the so-called green corrosion inhibitors, has started. Green corrosion inhibitors include natural plant-based products [1,2] and nontoxic man-made compounds such as, dyes [3–5], rare earth elements [6,7], Schiff bases [8–10] and medicines [11,12], which have been classified as environmentally friendly.

Extensive scientific research aimed at developing the new types of nontoxic corrosion inhibitors of aluminium has been going on for almost two decades [13]. Numerous hypotheses were elaborated about the mechanism of green corrosion inhibition in aluminium and its alloys in alkaline aqueous environments. It has been assumed that the aluminium corrosion deceleration mediated by green corrosion inhibitors depends on widening the pH stability range of amphoteric layers consisting of aluminium oxides and hydroxides; repairing/rebuilding of damaged oxide and hydroxide layers; decreasing the diffusion rates of reactive reagents to and from the metal's surface; and/or on removing the corrosion products from the surface of aluminium [14].

Typically, an active component is being extracted by using acids, organic solvents or water. The purification of plant extracts is often very tedious, labor-consuming and expensive. Moreover, the extraction method itself has certain disadvantages related to the use of the large volumes of organic solvents, which may have a negative impact on the environment. The main problem related to the use of plant extracts as green corrosion inhibitors results from their physicochemical stability under specific research conditions [15,16]. Also, the extraction of plant materials conducted at high temperatures can lead to the denaturation of active ingredients and, subsequently, to lowered efficacy of the extract. To this end, specifically designed synthesis reactions should be applied in which the substrates are inexpensive and environment-friendly, or other procedures based on one-step multicomponent reactions (MCRs) coupled to more energy-efficient and nonconventional methods of heating aided by ultrasound and microwave radiation [17–20].

The tendency to use plant extracts as corrosion inhibitors has yet another negative side, namely, the obtained extracts are mixtures of compounds, not pure chemicals. There have been rare attempts to phytochemically characterize some plant extracts. The efforts to identify the active components in plant

extracts are comparably infrequent. It is likely that the mixture of different chemical compounds can have a synergistic or antagonistic effect in relation to the inhibitory action of a given active component.

Many scientific studies have been dedicated to the analysis of the chemical composition of the bee products revealing their chemical complexity [21–25]. Janoskova et al. [26] studied the slug honey and identified 300 compounds belonging to various chemical classes (hydrocarbons, alcohols, ketones, terpenes and benzene derivatives). In particular, presence of numerous aliphatic dicarboxylic acids was identified in honey and bee pollen [27,28]. Such a wide spectrum of compounds displaying a potential anticorrosion activity drew the attention of scientists to the possible inhibitory properties of honey and other bee products.

Bee products were identified as efficient green inhibitors of corrosion in aluminium and its alloys. Rosliza et al. [29] researched the anticorrosive properties of natural honey applied to Al-Mg-Si alloy in seawater. The SEM analysis confirmed the presence of a thin layer of corrosion inhibitor on the surface of the protected alloy, which in effect decreased the overall rate of corrosion. Similar studies were reported by Gudić et al. [30]. The anticorrosion efficacy increased with increasing honey concentration, displaying various values for different honey types. For the analyzed range of honey concentrations, the maximum observed efficiency reached 81.7%. The polarization measurements presented in the aforementioned articles proved that the analyzed types of honey should be considered as mixed corrosion inhibitors displaying a higher impact on the anodic reaction. Gerengi et al. [31] demonstrated the influence of mad honey on the electrochemical properties of AA2007 aluminium alloy in 3.5% NaCl solution. Based on FTIR measurements, the authors identified active functional groups and chemical bonds, inter alia, C-O, C=O, C=C, C-H, -NH and –OH, involved in the creation of adsorption layer on the surface of the protected metal; the obtained results were in agreement with [29,30]. Similar conclusions were presented by Nik et al. [32] in their study based on AC/DC polarization methods. In all the cited examples, the adsorption processes followed the Langmuir model. The determined changes in Gibbs free energy suggest a physical mechanism of adsorption.

Until now, all the published reports focused on the inhibitory action of honey in relation to aluminium and its alloys in sodium chloride environment. Bee products not only consist of honey, but also include pollen, propolis and wax. After conducting a series of preliminary experiments, it has been decided that bee pollen possesses the best inhibitory properties in relation to aluminium corrosion under the aforementioned conditions. In the following study, we present the corrosion inhibition process of AA5754 in the bicarbonate buffer at pH 11. Based on the diverse but complementary electrochemical, analytical and physicochemical measurements, the mechanism of pollen activity as corrosion inhibitor is

discussed. Due to the fact that the bee products are mixtures of chemicals differing in composition and thus difficult to define unambiguously, a concurrent effort was undertaken to determine the groups of inhibitory compounds based on the independent studies of three fractions isolated from bee pollen via high performance liquid chromatography (HPLC). Water, water-ethanol, and dichloromethane were used as solvents during extraction procedure, the inhibition effect of the obtained products were examined.

2. Experimental

2.1. Sample

Metal specimens used in this study were made of AA5754 with a chemical composition (in wt.%) of 3.6% Mg, 0.5% Mn, 0.3% Fe, 0.3% Si, 0.1% Cr and the remainder Al. Its chemical constitution was confirmed based on Energy Dispersive X-Ray Spectroscopy (EDX) measurement. The samples were delivered in form of a rod, 10 mm in diameter, cut and prepared by grinding with abrasive papers 400-1800 grades and polished using diamond suspensions to obtain a mirror-like surface. Grinding and polishing were carried out on Digiprep 251 (Metkon, Turkey). The polished sample surfaces were cleaned using water and acetone and dried immediately. The specimen preparation procedure was performed according to ASTM G1-03 standard.

2.2. Preparation of corrosion inhibitor extracts

The mixture of 25g bee pollen was placed in a round bottom flask and mixed with 400 mL of 99.8% ethanol and water (1:1). Previously, the bee pollen was carefully homogenized with a mortar and pestle. The reaction mixture was stirred for 48 h at room temperature. The resulting mixture was then filtered, evaporated under reduced pressure, and finally dried over P_2O_5 to obtain 23.73 g of crude product with a yield of 94.93%. The crude product, denoted as INH1 extract, was used for further examination.

The INH1 extract (ethanol/water extract of bee pollen) was then dissolved in 200 mL of water and the aqueous phase was extracted three times with 200 mL of dichloromethane. The aqueous phase was evaporated under reduced pressure to obtain INH2 extract (water extract from INH1) with the 84.06% yield. The combined organic extracts were evaporated under reduced pressure and vacuum dried, resulting in INH3 extract (organic dichloromethane extract from INH1) with a yield of 2.87%. Water and ethanol have higher dipole moments compared to dichloromethane. The intermolecular interactions between solvent and soluble material effect solubility. Therefore, the amount of polar compounds that may have dissolved in INH1 and INH2 is higher compared to INH3.

4

The inhibitor extract was mixed with the bicarbonate buffer solution to form corrosive environment. The buffer was prepared using 227 cm^3 0.1 M NaOH and 500 cm^3 0.05 M NaHCO$_3$. The mixture was then diluted with deionized water to 1 L volume. The obtained buffer had pH 11 and the resistivity of 3.8 mScm^{-1}. Only the analytical purity Sigma Aldrich reagents were used for all procedures.

2.3. Corrosion studies

The mechanism of corrosion inhibitor adsorption can be determined on the basis of corrosion rate studies for the inhibitors displaying anodic and mixed protection mechanism [2,33,34]. Recently, an efficient approach to determining the adsorption isotherms through instantaneous impedance measurements in galvanostatic mode was proposed by Wysocka et al. [35,36]. The approach utilizes Dynamic Electrochemical Impedance Spectroscopy in galvanostatic mode (g-DEIS), a technique which has been successfully used to investigate highly non-stationary processes [37–43]. The g-DEIS measurements were carried out in the corrosion cell prior to and during the inhibitor injection in order to determine the dynamics of the adsorption process as well as its thermodynamic properties. Details of DEIS approach are presented elsewhere [37,44,45].

The measurement setup consisted of two cells connected by means of microflow peristaltic pump (Lead Fluid BQ80S, China). Initially, the volume in the corrosion cell, where the electrochemical measurements were conducted, was 3 mL and increased up to 5 mL throughout the measurement. The low cell volume was dictated by the low extraction efficiency of certain extracts, in this particular case of INH3. In order to avoid a significant variation of [Al(OH)$_4$]$^-$ concentration throughout the measurement, resulting from the corrosion of aluminium alloy in alkaline environment, the sample surface remaining in contact with electrolyte was 0.07 cm^2 [46]. The studied inhibitor in the amount of 0.1 g was dissolved in the buffer electrolyte in the preliminary cell. The inhibitor concentration in the corrosion cell varied in dependence on the peristaltic pump flow rate (0.02 mLmin^{-1}). A three-electrode setup was used, with AA5754 sample as the working electrode, platinum mesh as counter electrode and the silver rod covered with silver oxides serving as reference electrode (+0.174 V vs SHE). The sample was initially conditioned in the electrolyte in the absence of corrosion inhibitor for 1000 s (measurements started after 500 s), after which the inhibitor was pumped to the corrosion cell for the next 6000 s. The setup is shown in details elsewhere [36].

The system setup consisted of Autolab PGSTAT 128N galvanostat (Metrohm, Netherlands) connected to PXI-4464 measurement card for ac signal generation, and PXI-6124 card for AC/DC signal acquisition, both operating in PXIe-1073 chassis (all from National Instruments, USA). The g-DEIS

perturbation signal was composed of 29 superimposed elementary signals in the frequency range 4.5 kHz to 1 Hz, with 8 points per decade of frequency. Sampling frequency was 128 kHz. The amplitude of the perturbation signal was controlled to assure the response signal amplitude does not exceed 20 mV. The analysis window for the Fourier Transformation was 10 s in length. Similar operating parameters were successfully applied in the previous corrosion inhibitor studies [31,36].

The remaining corrosion studies, i.e. EIS and potentiodynamic polarization were carried out using the same three-electrode setup and in the corrosion cell. The measurements were performed on a Reference 600+ potentiostat (Gamry Instruments, USA) after the initial conditioning for 20 min. The polarization scans were recorded in the range between -0.25 V vs E_{corr} and +2.00 V vs Ag|Ag$_2$O, or until 10 mAcm^{-2} current density was reached. The scan rate was 2 mVs^{-1}. The EIS impedance measurements were carried out with frequency-response-analysis (FRA) under corrosion potential and perturbation signal frequency ranging between 100 kHz and 1 Hz, with the amplitude of 15 mV. The potentiodynamic polarization and EIS measurements were carried out at four different temperatures, namely 25, 35, 45 and 55 °C. During the measurements, the set temperature was kept constant by means of Corio thermostat (Julabo, Germany).

2.4. Physicochemical examination

Chemical analysis of bee pollen extracts: The Fourier Transform Infrared Spectroscopy (FTIR) measurements of the examined compounds were performed on a Bruker IFS 66 spectrometer using KBr pellet. Matrix Assisted Laser Desorption/Ionization - Time of Flight Mass Spectrometry (MALDI-TOF MS) experiments of all phases were carried out using a BIFLEX III TOF mass spectrometer (Bruker Daltonik, Germany). The chromatographic analysis (RP-HPLC) of dissolved samples was carried out using the Shimadzu HPLC system containing a UV/Vis wavelength detector. The C8 reverse-phase column (150 mm × 4.60 mm, particle size 3 μm, Phenomenex Luna C8, USA) was used for all samples. Eluent A: 0.1% trifluoroacetic acid (TFA) in water, Eluent B: 0.1% trifluoroacetic acid (TFA) in acetonitrile. All chromatograms were recorded at the column temperature of 25 °C using oven column, at wavelength of 250 nm with a linear gradient elution from 0% to 100% of eluent B with flow rate 1 mLmin^{-1} during 20 min.

Aluminium surface examination: The topography of AA5754 samples after the exposure to corrosive environment containing the studied inhibitor extracts was assessed by using a Scanning Electron Microscope equipped with a variable pressure chamber (VP-SEM) S-3400N (Hitachi, Japan) under the

6

accelerating voltage 20 kV. The SEM micrographs were recorded in back-scatter electron mode (BSE). The microscope was equipped with Energy Dispersive X-Ray Spectroscopy (EDX) detector UltraDry (ThermoFisher Scientific, USA) that had been used to chemically examine the analyzed alloy and the corrosion product layer.

High-resolution X-Ray Photoelectron Spectroscopy (XPS) was used to analyze the interactions of each corrosion inhibitor with the aluminium alloy surface in alkaline environment. The XPS measurements were performed by using an Escalab 250 Xi multispectroscope (ThermoFisher Scientific, USA). The spectroscope was equipped with an Al Kα X-Ray source, with a spot size of 250 μm. Measurements were carried out at 20 eV pass energy with charge compensation by means of a flood gun. The final calibration was performed by shifting the binding energy on spectral X-axis for peak characteristics of $Al2p_{3/2}$ metallic aluminium at 72.7 eV. The above value was measured on AA5754 reference sample prior to electrochemical studies.

3. Results and discussion

3.1. Characterization of the investigated bee pollen extracts

The FTIR spectroscopy studies were performed as the first step of the chemical and structural characterization of the obtained corrosion inhibitor extracts. In Fig. 1, the spectra of studied inhibitor extracts in the 4000 – 800 cm^{-1} range are presented. The peaks observed at 3360, 3010, and 3350 cm^{-1} for the respective samples INH1, INH2 and INH3 correspond to the stretching vibrations of -OH groups and hydrogen bond. The peaks in the 3010 – 2853 cm^{-1} region, which are also present in all the analyzed spectra, correspond to the stretching vibrations of -CH$_2$ or -CH$_3$ groups, while it is worth noting that only for INH1 and INH3 extracts another peak occur at ~3010 cm^{-1}, corresponding to stretching vibrations of –CH group [47,48]. Also, another characteristic peak occurring in all the spectra in the range between 1711 cm^{-1} and 1738 cm^{-1} corresponds to the stretching vibrations of C=O groups in ketones, aldehydes or esters. The peak observed at 1460 cm^{-1} is attributable to the -CH$_2$ or -CH$_3$ groups present in lipids [49]. Additionally, the absorption peak at ca. 1060 cm^{-1} that is present in all the spectra, most likely corresponds to carbohydrates. Due to the inability to isolate only one chemical component present in each fractions of analyzed bee pollen the above FTIR analyses identify the functional groups present in obtained extracts.

In the next step of bee pollen extract characterization, the quantitative analysis of all samples was conducted via HPLC technique. Analytical reversed-phase high-performance liquid chromatography (RP-HPLC) was performed with a C8 chromatography column thermostated in a column oven at 25 ºC.

All analyses were carried out in linear gradient. The absorbance was detected at 250 nm. All the extracts were dissolved in a mixture of ethanol/water at the 1:1 ratio. The obtained results (Fig. 2) directly indicate that all extracts were complex mixtures of chemical compounds. The ethanol/water extract of bee pollen, coded INH1, consisted of many compounds, while INH2 extract (after dissolution in aqueous phase and after extraction to dichloromethane) contained lesser amounts of nonpolar components. The reverse situation was observed in the case of INH3 extract, which had been obtained via dichloromethane extraction of INH1 extract. The INH3 extract contained significantly less polar compounds, while the nonpolar chemicals constituted the bulk of its total content. Polar molecules have areas of positive and negative electrical charge, which helps to make interaction with metal ions. The interaction potential for INH3 is lower than INH2 and INH1 and may affect the inhibition performance.

In the last step of chemical characterization of bee pollen extracts, the mass spectroscopy analysis was applied. The MALDI-TOF mass spectra were used to define the mass of individual components present in the analyzed corrosion inhibitors. For all experiments, 2,5-dihydroxybenzoic acid (DHB) was used as a matrix. The resulting MALDI-TOF mass spectra are shown in Fig. 3. The comparative spectral analysis of INH1 and INH2 extracts directly indicated that the analyzed samples were very similar with respect to molar mass. The mass spectra of INH1 and INH2 extracts revealed the four very intensive peaks at 497, 518, 519 and 688, additionally in all extracts the peak 788 is present. In INH3 extract (dichloromethane extract of INH1) the intensity of peak 688 is lower, while the intensity of peak 788 is higher, indicating the presence of chemical compounds corresponding to the above peaks is different. The lack of compounds exceeding value 1000 in any analyzed extract negates the presence of huge macromolecular compounds such as: proteins, peptides, oligosaccharides or nucleic acid fragments, which are most likely insoluble in the solvents used.

3.2. Inhibition efficiency offered by analyzed organic extracts

In order to determine the corrosion inhibition efficiency of the obtained bee pollen inhibitor extracts, the potentiodynamic polarization and electrochemical impedance spectroscopy studies were performed. The inhibitor concentration of 10 gL^{-1} was used in each case, and the measurements were carried out at 25 °C after the initial 15 min of conditioning in the electrolyte. The interaction of each inhibitor with the aluminium surface was compared by referring to the reference exposure of AA5754 alloy in bicarbonate buffer in the absence of corrosion inhibitor. The results of the aforementioned analysis are shown on Fig. 4a,b.

Each of the three investigated inhibitor extracts shifted the corrosion potential E_{corr} value towards anodic direction, which suggests the anodic mechanism of interaction or the mixed mechanism of interaction with the dominant anodic influence. The extrapolation of Tafel regions allowed the verification of a significant decrease in corrosion susceptibility of aluminium alloy resulting from the addition of INH1 extract. The inhibitor efficiency was assumed using corrosion current density j_{corr} values from the well-known relationship (1):

$$IE_{\%}^{(pol)} = \left(\frac{j_{corr}^0 - j_{corr}}{j_{corr}^0}\right) * 100\% \tag{1}$$

where j_{corr} and j_{corr}^0 refer to inhibited and uninhibited sample, respectively [50]. Nearly the same level of inhibition efficiency was provided by INH2 extract, which could be related to the similar molecular composition of both extracts. The corrosion inhibitor efficiency reached 93 and 88% for INH1 and INH2 extracts, respectively. On the other hand, while the addition of INH3 extract also appears to limit the corrosion rate due to the slowdown of the anodic process, the observed inhibitor efficiency was significantly lower, i.e. in the range of ~60% for 10 gL^{-1}.

The impedance data reveal a single time constant, thus the analysis was carried out using R(QR) electric equivalent circuit (EEC). The EEC utilized in all impedance measurements within the article was the modified Randles circuit. The applied modification concerns swapping the capacitor representing the combined double layer capacitance and adsorbed layer capacitance with the constant phase element (CPE). The CPE corresponds to the heterogeneous distribution of electrochemically active surface area on AA5754 sample, primarily due to its multiphase microstructure and the presence of local adsorption sites, in particular at low corrosion inhibitor concentrations [35,51,52]. The resistor in parallel to CPE represents the charge transfer resistance R_{CT}. The inductive loop observed for the reference sample should be ascribed to the intermediate adsorbed species, such as Al^+_{ads}, Al^{3+}_{ads} and OH^-_{ads} [46,53]. Their absence in case of inhibited samples testifies the decreased kinetics of metal dissolution.

Each investigated inhibitor offers good corrosion protection for aluminium in alkaline media, proven with significant increase in charge transfer resistance R_{CT}. The inhibition efficiency was directly calculated from R_{CT} changes with eq. (2):

$$IE_{\%}^{(EIS)} = \left(1 - \frac{R_{CT}^0}{R_{CT}}\right) * 100\% \tag{2}$$

where R_{CT} and R_{CT}^0 are measured for inhibited and uninhibited samples, respectively. It can be observed, that the lowest inhibition efficiency was obtained for the dichloromethane INH3 extract, rich in non-polar compounds. Thus, the EIS studies confirms the potentiodynamic polarization results.

An increase of the capacitive parameter was observed in the presence of any of the corrosion inhibitor. The effect results primarily from inhibitor impact on the capacitance dispersion, as manifested by drop of the CPE exponent. This parameter is strictly associated with surface homogeneity [54–56], corroborating altered appearance of the corrosion products layer verified by SEM (Fig. 5). For heterogeneous surfaces the effective double-layer capacitance C_{eff} can be estimated using eq. (3), based on Hirschorn approximation for surface time-constant distribution [57].

$$C_{eff} = Q^{1/n} \left(\frac{R_S R_{CT}}{R_S + R_{CT}} \right) \qquad (3)$$

The surface of AA5754 is covered with the corrosion products layer in each studied electrolyte, hence the comparable value of C_{eff}. The selected EEC offers a good fit to measured impedance data, with the χ^2-distribution not exceeding $6*10^{-4}$. The results of the analysis are summarized in Table 1.

The results obtained based on potentiodynamic polarization and impedance spectroscopy method may vary, in particular at lower inhibitor concentrations [36]. The difference originate from different method of system perturbation, but also susceptibility to change under the influence of non-stationary conditions and various data processing procedures. This factor was discussed in more detail in other work [35,58].

Regardless of the measurement approach, the inhibition efficiency of INH3 extract is lower. The INH3 extract was obtained with significantly lower yield. It had some compounds in common with both INH1 and INH2 extracts, but other chemicals were strictly separated. Taking into account the results of HPLC analysis, it can be concluded that the INH3 extract (organic dichloromethane extract from INH1) contains the compounds which moved to the organic layer and are more non-polar in relation to the INH1 extracts (ethanol/water extract of bee pollen) and INH2 extracts (water extract from INH1).

There is a possibility of synergistic corrosion inhibitor interaction between the compounds contained in INH2 and INH3 extracts, based on a slightly lower efficiency of INH2 in reference to the original INH1 extract. The high synergistic interaction between the various compounds present in complex organic extracts has been vastly reported in the literature [59–63].

3.3. Topography and surface chemistry of AA5754 due to the exposure

The topography of AA5754 alloy exposed for 18 hours to reference bicarbonate buffer (pH = 11) compared to buffer containing 10 gL^{-1} of studied corrosion inhibitor is presented in Figures 5a-d. The influence of aluminium alloys microstructure on its corrosion properties was topic of numerous studies [54,64–69]. The AA5754 contains a variety of intermetallic particles, composed of alloying additives not entirely soluble in the alloy matrix. The Mg-rich intermetallic particles present within this alloy include primarily Mg_2Si, but also Mg_2Al_3, both anodic with respect to the alloy matrix. These particles

10

easily oxidize even at mild conditions, however hydroxide $Mg(OH)_2$ and SiO_2*nH_2O deposits act as additional diffusion barrier for the corrosion process [64]. The second type of intermetallic particles, cathodic with respect to alloy matrix, is composed of $Al_6(Mn,Fe)$ and $Al_{15}(Mn,Fe)_3Si_2$ with exact stoichiometry depending on alloy composition [64,66,68]. These particles were marked with orange arrows on Fig. 5a-c. When exposed to oxidizing environment the alloy matrix corrodes surrounding the cathodic particles. The outcome on the BSE image is the slightly darker color of these areas due to higher intensity of metal oxides or adsorbed inhibitor.

The sample surface exposed to the reference buffer (Fig. 5a) is covered with a dense grid of micro-cracks, testifying the presence of the insoluble corrosion product layer, which starts to crack when dried under vacuum conditions of SEM. It can be observed that in the presence of INH1 extract (Fig. 5b) the surface of aluminium alloy is covered with a thicker layer of corrosion products and loosely spread large cracks. This observation allowed us to claim the limited corrosion rate of the corrosion product layer. The corrosive electrolyte appears to be affecting the aluminium sample the least after the addition of INH2 extract, as can be seen on the micrographs in Fig. 5c. The visible isolated cracks appear to be oriented around the intermetallic particles, which is in good agreement with their cathodic nature. The reduced number of cracks testifies for smaller thickness of the corrosion products layer or its lower hydration.

The topography of aluminium alloy exposed to INH3 extract (Fig. 5d) differs significantly. Similarly to the effect of solution containing INH1 or INH2, the sample surface became covered by the layer of corrosion products. Unlike the aforementioned electrolytes, adhesion of the corrosion product layer seems very low, and the layer's show local delamination in the form of sheets. Thus, the layer does not restrict the corrosion rate in a significant way. The surface underneath the delaminated areas is severely damaged and the phase structure is lost altogether. The surface is loosely covered with pits 5-10 μm in diameter, which could originated from detaching of intermetallic particles, however, the similar shape and size of caverns was linked by Wysocka et al. [46] to the hydrogen evolution sites on the aluminium surface. When comparing aluminium surface after exposure to INH3 with the reference sample, there is a possibility the compounds contained within this extract may limit the stability of the corrosion product layer accelerating the corrosion rate at low concentrations.

The adsorption of each investigated corrosion inhibitor on aluminium alloy surface was also studied using high-resolution XPS in the binding energy range of *C1s*, *O1s*, *N1s*, *Al2p*, *Mg1s* and *P2p* peaks. The results of XPS analysis are presented in Fig. 6. Besides the aforementioned elements, other notable

ones are sodium, chlorine, calcium and silicon, based on the XPS survey spectra. All elements but aluminium, magnesium and silicon originate from the bee pollen.

A peak deconvolution of each spectra was performed in order to determine the surface chemistry of aluminium alloy resulting from exposure to alkaline media in presence of the bee pollen extracts. The deconvolution results are summarized in Table 2. The primary element present on aluminium alloy surface after 18 h exposure to bicarbonate buffer (pH = 11) with addition of each inhibitor extract was carbon. The $C1s$ peak reveals rich surface chemistry, with four major peaks used for the deconvolution purposes. First of the aforementioned components, located at 284.6 eV should be ascribed to primarily aliphatic carbon C-C/C-H bonds, which may originate from the studied inhibitor but also adventitious carbon adsorbed on aluminium surface due to air exposure [70,71]. Secondly, the major component located at approx. 286.0 eV should be ascribed to various C-O bonds but also C-N bonds present in amines. The two remaining peaks, shifted by +1.5 and +2.8 eV with respect to the major component, correspond to ester/carbonyl and carboxyl functional groups respectively. A strong correlation can be seen between AA5754 samples exposed in the presence of INH1 and INH2 extracts, which both reveal higher amount of carbonyl and carboxyl functional groups, reaching nearly 40% of total carbon content with regard to 25% for INH3 extract. It is significant information taking into consideration that the carboxylic acids are found to be very strong corrosion inhibitors of aluminium in alkaline environments [72–74] and its presence in the corrosion product/adsorbed layer testifies the higher corrosion resistance.

Significant differences can be found analyzing $P2p_{3/2}$ peak (Fig. 6f), where phosphate functional group adsorption was confirmed resulting from Al-alloy exposure to INH1 and INH2 extracts. No peaks were found at 134.2 eV for INH3 extract. The presence of phosphorous in the bee pollen originates primarily from phospholipids [75]. Presence of phosphate groups is often connected to remarkable inhibition efficiency of aluminium in various electrolytes [73,76–79]. Thus, it may synergize with carboxylic acids contained within the bee pollen. Similar conclusion regarding corrosion activity of investigated electrolytes can be found based on $Al2p$ spectra (Fig. 6d). Here, the presence of nonstoichiometric corrosion products marked as Al-O$_{(2)}$ with $Al2p_{3/2}$ peak at approx. 76.0 eV was found to correlate with low corrosion resistance of aluminium [46,80]. On the other hand, Al-O$_{(1)}$ should be ascribed to Al_2O_3 passive layer. The thickness of the investigated layer exceeds 10 nm in each case; a conclusion drawn based on the lack of metallic $Al2p$ peak doublet in the analyzed spectra.

The oxygen $O1s$ peak was deconvoluted using three peak singlets, with model previously used to investigate the adsorption of organic corrosion inhibitors [36,81,82]. The main component, located at 532.7 eV is frequently attributed to the surface hydroxyl groups, but also oxygen in carbonyl or ester

groups within the adsorbed layer. Its share was found the most significant after exposure to INH2 extract. McCafferty and Wightman proposed a mathematic approach to further distinguish these species [83]. The second important component was located at 531.3 eV and attributed to metal oxide species O^{2-}, harmonizing with other works reporting approx. 1.5 eV shift between these two peaks. Finally, the last minor deconvoluted component was ascribed with the chemisorbed water within the corrosion product/adsorption layer and oxygen found in carboxyl functional groups [36,83,84]. Its content was the highest for INH1 and INH2 extracts, explaining cracks present within the layer as observed on SEM images (Fig. 5a,b). The amount of chemisorbed water is reported to be higher for actively corroding samples due to hydration of nonstoichiometric corrosion products, yet low presence in Al exposed to INH3 extract may be explained by lower amount of adsorbed carbonyl and carboxyl species.

The primary similarities between each analyzed spectra concerned the chemistry of measured *N1s* (Fig. 6c) and *Mg1s* (Fig. 6e) components. The nitrogen found in each analyzed spectra did not exceed 2 at.%, in each case consisting of two deconvoluted peaks, most likely representing amino acids (BE ~ 400.2 eV) and N-oxides (BE ~401.7 eV) [85]. Due to low concentration it is assumed to have negligible influence on inhibition efficiency. The analyzed magnesium being the primary alloy additive of this type of alloys, was found in the energy range characteristic for magnesium hydroxides.

3.4. Adsorption mechanism of bee pollen extracts

The primary approach to determining the adsorption mechanism of the applied corrosion inhibitor is based on the construction of an adsorption isotherms. While numerous models are used to study the corrosion processes, i.e. Frumkin [86,87], Freundlich [88,89], Temkin [88,90], Flory-Huggins [91] and others [92], in most cases the simplest Langmuir model of adsorption is applied [31,89,93,94]. In the case of bee pollen extracts, the excessive complexity of the model is not advised because under electrolytic conditions the resulting isotherm depends on all the occurring processes (i.e. sorption, hydration, dissolution). The proper control of each individual factor is impossible in such a complex environment.

In the corrosion studies, it is assumed that the surface coverage θ responds to the inhibitor efficiency $IE_\%$. On the other hand, the inhibitor efficiency may be determined from the changes in instantaneous charge transfer resistance R_{CT} throughout the inhibitor injection experiment by using eq. (2). Performing g-DEIS measurements allows the determination of instantaneous impedance spectra, where the charge transfer resistance value can be drawn based on an appropriate electric equivalent circuit (EEC) selection. The measurements should be carried out in the galvanostatic mode under zero current

conditions because the injection of the anodic corrosion inhibitor significantly influences the value of corrosion potential, as shown in Fig. 4a. Thus, an artificial polarization factor will be introduced during the inhibitor injection if the measurements are carried out in the potentiostatic mode [36,95]. The exemplary g-DEIS results, obtained during the injection experiment for INH2 and INH3 extracts, are shown in Fig. 7a. The instantaneous values of charge transfer resistance R_{CT} were estimated from the impedance data using R(QR) EEC. Its course of changes over the experiment duration is presented in Fig. 7b, while Fig. 7c reveals the resulting instantaneous change of surface coverage θ.

We have confirmed that the bee pollen extracts follow the Langmuir adsorption isotherm model, which is also in good agreement with previously published reports on other bee products. According to the Langmuir adsorption isotherm model, the adsorption equilibrium constant K_{ads} can be described by equation (4):

$$K_{ads}c = \left(\frac{\theta}{1-\theta}\right) \tag{4}$$

where c is the corrosion inhibitor concentration. The Langmuir isotherm can be rearranged in the form of linear equation, as presented in eq. (5) [30,96].

$$\frac{c}{\theta} = \frac{1}{K_{ads}} + c \tag{5}$$

The above described approach is particularly useful for representing complex inhibitor extracts, where the exact average molar masses of the inhibitor molecules are unknown, such as in this case [97–100].

The Langmuir adsorption isotherms for all the studied inhibitors were constructed based on g-DEIS measurements, as presented in Fig. 8. A clear similarity between the slopes of INH1 and INH2 adsorption isotherms can be observed for all the analyzed inhibitor concentrations. The adsorption isotherm drawn as a result of INH3 extract addition is the only one that does not follow the Langmuir adsorption model. In the case of INH3 extract, the asymptotic character of c/θ=f(c) function originates from the fact that at low extract concentrations, INH3 does not lowers the corrosion rate; actually, the catalytic impact on aluminium corrosion was noted. The observed situation could have possibly occurred due to insufficient concentration of anodic inhibitor resulting from the active-passive cell formation. Furthermore, the delamination visible on the SEM micrograph in Fig. 4c might have originated from the presence of such an active-passive cell. The slope values of the constructed adsorption isotherms confirm the occurrence of similar interaction mechanisms in the case of water INH2 extract and ethanol INH1 extract.

The adsorption equilibrium constant K_{ads}, estimated from the isotherm slope, can be used to predict Gibbs free energy ΔG^{*} for the interaction of INH1 and INH2 extracts with the aluminium surface using eq. (6):

$$K_{ads} = \frac{1}{c_{H_2O}} exp\left(\frac{-\Delta G^*}{RT}\right) \qquad (6)$$

where c_{H_2O} is the molar concentration of water (55.5 M), while R and T have their usual meaning.

The estimated values of ΔG^* once again confirmed the hypothesis of shared adsorption mechanism between INH1 and INH2 extracts (see the summary of results in Table 3). The negative Gibbs energy in each analyzed case suggests the spontaneous adsorption of active compounds present in the bee pollen extract, serving as corrosion inhibitors. It also explains the successive increase in inhibition efficiency with increasing extract concentration. The ΔG^* values between -4 and -6 kJmol^{-1} were recorded for both INH1 and INH2 extracts, being a clear indication of the physisorption mechanism. The physical adsorption is said to be a dominant mechanism of adsorption process for $\Delta G^* > - 20$ kJmol^{-1} [36,101,102]. Significantly more negative ΔG^* values suggest the chemical adsorption mechanism. Furthermore, due to the aforementioned similarity, a claim can be made that the species contained within the analyzed bee pollen and responsible for its enhanced corrosion inhibition efficiency are more likely to be found in INH2 extract rather than in INH3. On the other hand, the compounds present in INH3 extract require significantly higher concentrations in order to provide anticorrosion protection of aluminium. However, at such high concentrations, their inhibition efficiency is on par with those of other extracts (refer to Fig. 7c).

The effect of physisorption mechanism manifests itself by a decrease in the inhibitor efficiency with increasing temperature of electrolyte. This is said to be due to inhomogeneous adsorption process, where the adsorbed inhibitor energetically blocks only some of the active sites on the metal surface, isolating them. Other active sites, which display higher activation energy, will still take part in the corrosion process [103,104]. The relationship between the corrosion rate [CR] and temperature can be regarded as an Arrhenius-type process. Thus, carrying out the measurements in a wide temperature range not only allows the determination of thermodynamic functions in relation to activation entropy ΔS_a^* and activation enthalpy ΔH_a^*, but also facilitates the calculation of thermal stability of the investigated compounds. The aforementioned parameters can be evaluated based on eq. (7) [105–107].

$$ln\left(\frac{[CR]}{T}\right) = \left[ln\left(\frac{R}{Nh}\right) + \frac{\Delta S_a^*}{R}\right] - \frac{\Delta H_a^*}{RT} \qquad (7)$$

where N is Avogadro's number and h is Plank's constant.

The Arrhenius plots for AA5754 with and without addition of 10 gL^{-1} of corrosion inhibitor extracts are presented in Fig. 9 for a temperature range between 25 and 55 °C, while the estimated values of the aforementioned kinetic and thermodynamic parameters characterizing the adsorption process are shown

in Table 3. The corrosion rate [CR] was calculated based on corrosion current density j_0 using the Faraday's law. The value j_0 was estimated with EIS from R_{CT} using eq. (8).

$$j_0 = \frac{RT}{nFR_{CT}}$$

(8)

The ΔS_a^* and ΔH_a^* were both estimated based on the impedance rather than potentiodynamic polarization studies to unify the obtained results with ΔG^*. Various approaches may, however, lead to discrepancies of measured corrosion rate values.

It should be noted that the increase in the corrosion rate with increasing temperature was similar, while the INH3 extract appears to have lost all of its anticorrosion properties at a temperature of 55 °C. The inhibition efficiency values of the remaining extracts revealed a similar tendency, although the high efficiencies were retained even at the most elevated temperatures. In comparison, the corrosion rate of aluminium sample in a buffer solution in the absence of corrosion inhibitor was the least affected by varying temperature, which should be related to the diffusion control of the oxidation process.

In each studied electrolyte, including the reference bicarbonate buffer without the corrosion inhibitor, the corrosion process was exothermic, as verified by the negative value of ΔH_a^*. The value of the discussed parameter between -27 and -29 kJmol^{-1} was similar for each studied corrosion inhibitor interaction. The absolute value of enthalpy below 40 kJmol^{-1} is characteristic feature for the physisorption processes. While both physical and chemical adsorption mechanisms may be characterized by the negative values of ΔH_a^*, it is only chemisorption process that displays positive ΔH_a^*value [108,109].

The analysis of entropy values ΔS_a^* of the investigated corrosion inhibitors revealed that they increased significantly and became positive in comparison to the reference buffer. The lowest value of ΔS_a^* among extracts was recorded for INH2, while the highest value was achieved for INH1 and INH3 extracts. It is claimed that the entropy increase in the presence of inhibitor should be connected to the increase in disorder resulting from the transformation of reactants into an activated complex [108–110].

4. Conclusions

We have investigated the corrosion inhibition efficiency of bee pollen extracts in relation to aluminium in alkaline media (bicarbonate buffer, pH = 11). There are few hundreds various compounds reported to be present in the melliferous products while significant amount may successfully lower the corrosion rate of aluminum in the studied environment. In this work, we made an attempt to distinguish the inhibitor-active compounds in such complex mixtures by comparison of the inhibition efficiency and the

16

adsorption mechanism of corrosion inhibitor extracts obtained via extraction in water/ethanol (INH1), water (INH2) and dichloromethane (INH3).

We demonstrated the high resemblance of INH2 aqueous extract to the original material, while INH3 extract was characterized with lower inhibition efficiency, even negative at low concentrations. We have also shown the synergistic interaction between the corrosion inhibitors in INH2 and INH3 extracts. The application of g-DEIS approach during the controlled injection of a given inhibitor allowed for the accurate determination of Gibbs free energy and the confirmation of the spontaneous adsorption of each inhibitor. Both INH1 and INH2 extracts followed the Langmuir adsorption mechanism, while the course of INH3 isotherm was significantly different. In each studied case, we have also confirmed the physical mechanism of adsorption via electrostatic interaction. The altered interaction of INH3 extract might be possibly related to the complex formation of active compounds.

The analytical and physicochemical studies of the obtained extracts brought valuable information regarding their composition. The mass spectrometry measurements supplied the clear marker regarding the atomic mass of separated compounds, which did not exceed 1000 negating possible presence of huge peptides, oligosaccharides or nucleic acid fragments. The HPLC analysis allowed us to bring the conclusion regarding significantly higher amount of non-polar compounds in the INH3 extract, bound with the separation method. The extraction yield of this extract was also the lowest.

The FTIR analysis verified the presence of carbohydrates, ketones, aldehydes and/or esters, carboxylic acids as well as phospholipids within analyzed extracts. The XPS examination of AA5754 surface allowed to confirm much stronger interaction of species containing carboxyl and carbonyl functional groups with the metal surface in the case of INH1 and INH2 extracts. Furthermore, the INH3-exposed sample was the only one where the phosphate groups were not found by XPS.

While we cannot unambiguously state the exact compounds responsible for the high inhibition efficiency of the bee pollen extracts, this feature should be connected in particular with carboxylic acids and phospholipids based on our findings. The next suggested step is to attempt the separation, crystallization and characterization of some of these chemicals.

5.   Acknowledgments

6. References

[1] N. Raghavendra, J.I. Bhat, Anti-corrosion Properties of Areca Palm Leaf Extract on Aluminium in 0.5 M HCl Environment, South Afr. J. Chem. 71 (2018) 30–38. doi:10.17159/0379-4350/2018/v71a4.

[2] N. Chaubey, V.K. Singh, M.A. Quraishi, Electrochemical approach of Kalmegh leaf extract on the corrosion behavior of aluminium alloy in alkaline solution, Int. J. Ind. Chem. 8 (2017) 75–82. doi:10.1007/s40090-016-0103-y.

[3] E.E. Oguzie, Corrosion inhibition of mild steel in hydrochloric acid solution by methylene blue dye, Mater. Lett. 59 (2005) 1076–1079. doi:10.1016/j.matlet.2004.12.009.

[4] E.E. Oguzie, Inhibiting effect of crystal violet dye on aluminium corrosion in acidic and alkaline media, Chem. Eng. Commun. 196 (2008) 591–601. doi:10.1080/00986440802483848.

[5] E.E. Oguzie, G.N. Onuoha, A.I. Onuchukwu, The inhibition of aluminium corrosion in potassium hydroxide by "Congo Red" dye, and synergistic action with halide ions, Anti-Corros. Methods Mater. 52 (2005) 293–298. doi:10.1108/00035590510615794.

[6] T.J. Haley, Pharmacology and Toxicology of the Rare Earth Elements, J. Pharm. Sci. 54 (1965) 663–670. doi:10.1002/jps.2600540502.

[7] M. Bethencourt, F.J. Botana, J.J. Calvino, M. Marcos, M.A. Rodrı́guez-Chacón, Lanthanide compounds as environmentally-friendly corrosion inhibitors of aluminium alloys: a review, Corros. Sci. 40 (1998) 1803–1819. doi:10.1016/S0010-938X(98)00077-8.

[8] H. Ju, Z.-P. Kai, Y. Li, Aminic nitrogen-bearing polydentate Schiff base compounds as corrosion inhibitors for iron in acidic media: A quantum chemical calculation, Corros. Sci. 50 (2008) 865–871. doi:10.1016/j.corsci.2007.10.009.

[9] I. Ahamad, R. Prasad, M.A. Quraishi, Thermodynamic, electrochemical and quantum chemical investigation of some Schiff bases as corrosion inhibitors for mild steel in hydrochloric acid solutions, Corros. Sci. 52 (2010) 933–942. doi:10.1016/j.corsci.2009.11.016.

[10] R. Solmaz, E. Altunbaş, G. Kardaş, Adsorption and corrosion inhibition effect of 2-((5-mercapto-1,3,4-thiadiazol-2-ylimino)methyl)phenol Schiff base on mild steel, Mater. Chem. Phys. 125 (2011) 796–801. doi:10.1016/j.matchemphys.2010.09.056.

[11] M.M. El-Naggar, Corrosion inhibition of mild steel in acidic medium by some sulfa drugs compounds, Corros. Sci. 49 (2007) 2226–2236. doi:10.1016/j.corsci.2006.10.039.

[12] G. Gece, Drugs: A review of promising novel corrosion inhibitors, Corros. Sci. 53 (2011) 3873–3898. doi:10.1016/j.corsci.2011.08.006.

[13] K. Xhanari, M. Finšgar, M. Knez Hrnčič, U. Maver, Ž. Knez, B. Seiti, Green corrosion inhibitors for aluminium and its alloys: a review, RSC Adv. 7 (2017) 27299–27330. doi:10.1039/C7RA03944A.

[14] F. Mansfeld, ed., Corrosion mechanisms, M. Dekker, New York, 1987.

[15] A.K. Maayta, N.A.F. Al-Rawashdeh, Inhibition of acidic corrosion of pure aluminum by some organic compounds, Corros. Sci. 46 (2004) 1129–1140. doi:10.1016/j.corsci.2003.09.009.

[16] M. Aliofkhazraei, Developments in corrosion protection, INTECH, Rijeka, Croatia, 2014.

[17] A. Dömling, Recent Developments in Isocyanide Based Multicomponent Reactions in Applied Chemistry [†], Chem. Rev. 106 (2006) 17–89. doi:10.1021/cr0505728.

[18] M.S. Singh, S. Chowdhury, Recent developments in solvent-free multicomponent reactions: a perfect synergy for eco-compatible organic synthesis, RSC Adv. 2 (2012) 4547. doi:10.1039/c2ra01056a.

[19] R.C. Cioc, E. Ruijter, R.V.A. Orru, Multicomponent reactions: advanced tools for sustainable organic synthesis, Green Chem. 16 (2014) 2958–2975. doi:10.1039/C4GC00013G.

[20] C. Capello, U. Fischer, K. Hungerbühler, What is a green solvent? A comprehensive framework for the environmental assessment of solvents, Green Chem. 9 (2007) 927. doi:10.1039/b617536h.

[21] M.V. Baroni, M.L. Nores, M.D.P. Díaz, G.A. Chiabrando, J.P. Fassano, C. Costa, D.A. Wunderlin, Determination of Volatile Organic Compound Patterns Characteristic of Five Unifloral Honey by Solid-Phase Microextraction–Gas Chromatography–Mass Spectrometry Coupled to Chemometrics, J. Agric. Food Chem. 54 (2006) 7235–7241. doi:10.1021/jf061080e.

[22] L. Yaoa, Y. Jiang, R. Singanusong, N. Datta, K. Raymont, Phenolic acids in Australian Melaleuca, Guioa, Lophostemon, Banksia and Helianthus honeys and their potential for floral authentication, Food Res. Int. 38 (2005) 651–658. doi:10.1016/j.foodres.2005.01.002.

[23] F.A. Tomás-Barberán, I. Martos, F. Ferreres, B.S. Radovic, E. Anklam, HPLC flavonoid profiles as markers for the botanical origin of European unifloral honeys: HPLC flavonoid profiles as unifloral honey markers, J. Sci. Food Agric. 81 (2001) 485–496. doi:10.1002/jsfa.836.

[24] G. Bergamo, S.K. Tischer Seraglio, L.V. Gonzaga, R. Fett, A.C.O. Costa, Mineral profile as a potential parameter for verifying the authenticity of bracatinga honeydew honeys, LWT. 97 (2018) 390–395. doi:10.1016/j.lwt.2018.07.028.

[25] L. Fearnley, D.R. Greenwood, M. Schmitz, J.M. Stephens, R.C. Schlothauer, K.M. Loomes, Compositional analysis of manuka honeys by high-resolution mass spectrometry: Identification of a manuka-enriched archetypal molecule, Food Chem. 132 (2012) 948–953. doi:10.1016/j.foodchem.2011.11.074.

[26] N. Janoskova, O. Vyviurska, I. Špánik, Identification of volatile organic compounds in honeydew honeys using comprehensive gas chromatography, J. Food Nutr. Res. 53 (2014) 353–362.

[27] Echigo T., Takenaka T., Production of Organic Acids in Honey by Honeybees, J. Agric. Chem. Soc. Jpn. 48 (1974) 225–230. doi:10.1271/nogeikagaku1924.48.225.

[28] A.L. Wilkins, Y. Lu, Extractives from New Zealand Honeys. 5. Aliphatic Dicarboxylic Acids in New Zealand Rewarewa (Knightea excelsa) Honey, J. Agric. Food Chem. 43 (1995) 3021–3025. doi:10.1021/jf00060a006.

[29] R. Rosliza, W.B. Wan Nik, S. Izman, Y. Prawoto, Anti-corrosive properties of natural honey on Al–Mg–Si alloy in seawater, Curr. Appl. Phys. 10 (2010) 923–929. doi:10.1016/j.cap.2009.11.074.

[30] S. Gudić, L. Vrsalović, M. Kliškić, I. Jerković, A. Radonić, M. Zekić, Corrosion Inhibition of AA 5052 Aluminium Alloy in NaCl Solution by Different Types of Honey, Int J Electrochem Sci. 11 (2016) 998–1011.

[31] H. Gerengi, H. Goksu, P. Slepski, The inhibition effect of mad Honey on corrosion of 2007-type aluminium alloy in 3.5% NaCl solution, Mater. Res. 17 (2014) 255–264. doi:10.1590/S1516-14392013005000174.

[32] W.W.B. Nik, M.F. Zulkifli, R. Rosliza, M.J. Ghazali, K.F. Khaled, Potential of honey as corrosion inhibitor for aluminium alloy in seawater, World Appl. Sci. J. 14 (2011) 215–220.

[33] A. Singh, I. Ahamad, M.A. Quraishi, Piper longum extract as green corrosion inhibitor for aluminium in NaOH solution, Arab. J. Chem. 9 (2016) S1584–S1589. doi:10.1016/j.arabjc.2012.04.029.

[34] J. Wang, A. Singh, M. Talha, X. Luo, X. Deng, L. Yuanhua, Electrochemical and Theoretical Study of Imidazole Derivative as Effective Corrosion Inhibitor for Aluminium, Int. J. Electrochem. Sci. (2018) 11539–11548. doi:10.20964/2018.12.44.

[35] J. Wysocka, M. Cieslik, S. Krakowiak, J. Ryl, Carboxylic acids as efficient corrosion inhibitors of aluminium alloys in alkaline media, Electrochimica Acta. 289 (2018) 175–192. doi:10.1016/j.electacta.2018.08.070.

[36] J. Wysocka, S. Krakowiak, J. Ryl, Evaluation of citric acid corrosion inhibition efficiency and passivation kinetics for aluminium alloys in alkaline media by means of dynamic impedance monitoring, Electrochimica Acta. 258 (2017) 1463–1475. doi:10.1016/j.electacta.2017.12.017.

[37] K. Darowicki, P. Ślepski, Dynamic electrochemical impedance spectroscopy of the first order electrode reaction, J. Electroanal. Chem. 547 (2003) 1–8. doi:10.1016/S0022-0728(03)00154-2.

[38] J. Ryl, R. Bogdanowicz, P. Slepski, M. Sobaszek, K. Darowicki, Dynamic Electrochemical Impedance Spectroscopy (DEIS) as a Tool for Analyzing Surface Oxidation Processes on Boron-Doped Diamond Electrodes, J. Electrochem. Soc. 161 (2014) H359–H364. doi:10.1149/2.016406jes.

[39] K. Darowicki, S. Krakowiak, P. Slepski, The time dependence of pit creation impedance spectra, Electrochem. Commun. 6 (2004) 860–866. doi:10.1016/j.elecom.2004.06.010.

[40] H. Gerengi, K. Darowicki, P. Slepski, G. Bereket, J. Ryl, Investigation effect of benzotriazole on the corrosion of brass-MM55 alloy in artificial seawater by dynamic EIS, J. Solid State Electrochem. 14 (2010) 897–902. doi:10.1007/s10008-009-0923-1.

[41] K. Darowicki, A. Zieliński, K. J Kurzydłowski, Application of dynamic impedance spectroscopy to atomic force microscopy, Sci. Technol. Adv. Mater. 9 (2008) 045006. doi:10.1088/1468-6996/9/4/045006.

[42] A.S. Bondarenko, I.E.L. Stephens, H.A. Hansen, F.J. Pérez-Alonso, V. Tripkovic, T.P. Johansson, J. Rossmeisl, J.K. Nørskov, I. Chorkendorff, The Pt(111)/Electrolyte Interface under Oxygen Reduction Reaction Conditions: An Electrochemical Impedance Spectroscopy Study, Langmuir. 27 (2011) 2058–2066. doi:10.1021/la1042475.

[43] B.B. Berkes, A. Maljusch, W. Schuhmann, A.S. Bondarenko, Simultaneous Acquisition of Impedance and Gravimetric Data in a Cyclic Potential Scan for the Characterization of Nonstationary Electrode/Electrolyte Interfaces, J. Phys. Chem. C. 115 (2011) 9122–9130. doi:10.1021/jp200755p.

[44] P. Slepski, K. Darowicki, E. Janicka, G. Lentka, A complete impedance analysis of electrochemical cells used as energy sources, J. Solid State Electrochem. 16 (2012) 3539–3549. doi:10.1007/s10008-012-1825-1.

[45] K. Darowicki, Theoretical description of the measuring method of instantaneous impedance spectra, J. Electroanal. Chem. 486 (2000) 101–105. doi:10.1016/S0022-0728(00)00110-8.

[46] J. Wysocka, S. Krakowiak, J. Ryl, K. Darowicki, Investigation of the electrochemical behaviour of AA1050 aluminium alloy in aqueous alkaline solutions using Dynamic Electrochemical Impedance Spectroscopy, J. Electroanal. Chem. 778 (2016) 126–136. doi:10.1016/j.jelechem.2016.08.028.

[47] P. Larkin, Infrared and raman spectroscopy: principles and spectral interpretation, Elsevier, Amsterdam ; Boston, 2011.

[48] A.H. Al-Moubaraki, A.A. Al-Howiti, M.M. Al-Dailami, E.A. Al-Ghamdi, Role of aqueous extract of celery (Apium graveolens L.) seeds against the corrosion of aluminium/sodium hydroxide systems, J. Environ. Chem. Eng. 5 (2017) 4194–4205. doi:10.1016/j.jece.2017.08.015.

[49] B. Stuart, Infrared spectroscopy: fundamentals and applications, J. Wiley, Chichester, West Sussex, England ; Hoboken, NJ, 2004.

[50] Z. Moghadam, M. Shabani-Nooshabadi, M. Behpour, Electrochemical performance of aluminium alloy in strong alkaline media by urea and thiourea as inhibitor for aluminium-air batteries, J. Mol. Liq. 242 (2017) 971–978. doi:10.1016/j.molliq.2017.07.119.

[51] G. Moretti, F. Guidi, G. Grion, Tryptamine as a green iron corrosion inhibitor in 0.5 M deaerated sulphuric acid, Corros. Sci. 46 (2004) 387–403. doi:10.1016/S0010-938X(03)00150-1.

[52] D.A. López, S.N. Simison, S.R. de Sánchez, The influence of steel microstructure on CO2 corrosion. EIS studies on the inhibition efficiency of benzimidazole, Electrochimica Acta. 48 (2003) 845–854. doi:10.1016/S0013-4686(02)00776-4.

[53] D.D. Macdonald, Evaluation of Alloy Anodes for Aluminum-Air Batteries, J. Electrochem. Soc. 135 (1988) 2410. doi:10.1149/1.2095348.

[54] J. Ryl, J. Wysocka, M. Jarzynka, A. Zielinski, J. Orlikowski, K. Darowicki, Effect of native air-formed oxidation on the corrosion behavior of AA 7075 aluminum alloys, Corros. Sci. 87 (2014) 150–155. doi:10.1016/j.corsci.2014.06.022.

[55] J. Tymoczko, W. Schuhmann, A.S. Bandarenka, The constant phase element reveals 2D phase transitions in adsorbate layers at the electrode/electrolyte interfaces, Electrochem. Commun. 27 (2013) 42–45. doi:10.1016/j.elecom.2012.11.001.

[56] H. Gerengi, H.I. Sahin, *Schinopsis lorentzii* Extract As a Green Corrosion Inhibitor for Low Carbon Steel in 1 M HCl Solution, Ind. Eng. Chem. Res. 51 (2012) 780–787. doi:10.1021/ie201776q.

[57] B. Hirschorn, M.E. Orazem, B. Tribollet, V. Vivier, I. Frateur, M. Musiani, Determination of effective capacitance and film thickness from constant-phase-element parameters, Electrochimica Acta. 55 (2010) 6218–6227. doi:10.1016/j.electacta.2009.10.065.

[58] J. Orlikowski, J. Ryl, M. Jarzynka, S. Krakowiak, K. Darowicki, Instantaneous Impedance Monitoring of Aluminum Alloy 7075 Corrosion in Borate Buffer with Admixed Chloride Ions, CORROSION. 71 (2015) 828–838. doi:10.5006/1546.

[59] S.A. Umoren, M.M. Solomon, Synergistic corrosion inhibition effect of metal cations and mixtures of organic compounds: A Review, J. Environ. Chem. Eng. 5 (2017) 246–273. doi:10.1016/j.jece.2016.12.001.

[60] J. Zhao, G. Chen, The synergistic inhibition effect of oleic-based imidazoline and sodium benzoate on mild steel corrosion in a CO2-saturated brine solution, Electrochimica Acta. 69 (2012) 247–255. doi:10.1016/j.electacta.2012.02.101.

[61] R. Fuchs-Godec, Effects of surfactants and their mixtures on inhibition of the corrosion process of ferritic stainless steel, Electrochimica Acta. 54 (2009) 2171–2179. doi:10.1016/j.electacta.2008.10.014.

[62] Y. Qiang, L. Guo, S. Zhang, W. Li, S. Yu, J. Tan, Synergistic effect of tartaric acid with 2,6-diaminopyridine on the corrosion inhibition of mild steel in 0.5 M HCl, Sci. Rep. 6 (2016). doi:10.1038/srep33305.

[63] R.T. Loto, Corrosion Inhibition Performance of the Synergistic Effect of Rosmarinus officinalis and 5-Bromovanillin on 1018 Carbon Steel in Dilute Acid Media, J. Fail. Anal. Prev. 17 (2017) 1031–1043. doi:10.1007/s11668-017-0334-z.

[64] K.A. Yasakau, M.L. Zheludkevich, S.V. Lamaka, M.G.S. Ferreira, Role of intermetallic phases in localized corrosion of AA5083, Electrochimica Acta. 52 (2007) 7651–7659. doi:10.1016/j.electacta.2006.12.072.

[65] J. Wloka, G. Bürklin, S. Virtanen, Influence of second phase particles on initial electrochemical properties of AA7010-T76, Electrochimica Acta. 53 (2007) 2055–2059. doi:10.1016/j.electacta.2007.09.004.

[66] R. Goswami, G. Spanos, P.S. Pao, R.L. Holtz, Precipitation behavior of the ß phase in Al-5083, Mater. Sci. Eng. A. 527 (2010) 1089–1095. doi:10.1016/j.msea.2009.10.007.

[67] Y. Huang, Y. Li, Z. Xiao, Y. Liu, Y. Huang, X. Ren, Effect of homogenization on the corrosion behavior of 5083-H321 aluminum alloy, J. Alloys Compd. 673 (2016) 73–79. doi:10.1016/j.jallcom.2016.02.228.

[68] A. Afseth, J.H. Nordlien, G.M. Scamans, K. Nisancioglu, Influence of heat treatment and surface conditioning on filiform corrosion of aluminium alloys AA3005 and AA5754, Corros. Sci. 43 (2001) 2359–2377. doi:10.1016/S0010-938X(01)00019-1.

[69] C. Illoul, N. Zazi, F. Debiane, J.-P. Chopart, Relation Between Mechanical Instabilities and Corrosion Sensitivity of Aluminum Body Cans Surfaces, Prot. Met. Phys. Chem. Surf. 54 (2018) 876–883. doi:10.1134/S2070205118050106.

[70] H. Piao, N.S. McIntyre, Adventitious carbon growth on aluminium and gold-aluminium alloy surfaces, Surf. Interface Anal. 33 (2002) 591–594. doi:10.1002/sia.1425.

[71] T.L. Barr, S. Seal, Nature of the use of adventitious carbon as a binding energy standard, J. Vac. Sci. Technol. Vac. Surf. Films. 13 (1995) 1239–1246. doi:10.1116/1.579868.

[72] B. Müller, Citric acid as corrosion inhibitor for aluminium pigment, Corros. Sci. 46 (2004) 159–167. doi:10.1016/S0010-938X(03)00191-4.

[73] J. Qu, G. Chen, H. Wang, D. Nie, Effect of water content on corrosion inhibition behavior of self-assembled TDPA on aluminum alloy surface, Trans. Nonferrous Met. Soc. China. 23 (2013) 3137–3144. doi:10.1016/S1003-6326(13)62844-7.

[74] A.R. Madram, F. Shokri, M.R. Sovizi, H. Kalhor, Aromatic Carboxylic Acids as Corrosion Inhibitors for Aluminium in Alkaline Solution:, Port. Electrochimica Acta. 34 (2016) 395–405. doi:10.4152/pea.201606395.

[75] K. Komosinska-Vassev, P. Olczyk, J. Kaźmierczak, L. Mencner, K. Olczyk, Bee Pollen: Chemical Composition and Therapeutic Application, Evid. Based Complement. Alternat. Med. 2015 (2015) 1–6. doi:10.1155/2015/297425.

[76] K. Xhanari, M. Finšgar, Organic corrosion inhibitors for aluminum and its alloys in chloride and alkaline solutions: A review, Arab. J. Chem. (2016). doi:10.1016/j.arabjc.2016.08.009.

[77] Y.I. Kuznetsov, Organic corrosion inhibitors: where are we now? A review. Part IV. Passivation and the role of mono- and diphosphonates, Int. J. Corros. Scale Inhib. 6 (2017). doi:10.17675/2305-6894-2017-6-4-3.

[78] K. Wapner, M. Stratmann, G. Grundmeier, Structure and stability of adhesion promoting aminopropyl phosphonate layers at polymer/aluminium oxide interfaces, Int. J. Adhes. Adhes. 28 (2008) 59–70. doi:10.1016/j.ijadhadh.2007.05.001.

[79] H. Allal, Y. Belhocine, E. Zouaoui, Computational study of some thiophene derivatives as aluminium corrosion inhibitors, J. Mol. Liq. 265 (2018) 668–678. doi:10.1016/j.molliq.2018.05.099.

[80] L. Kobotiatis, N. Pebere, P.G. Koutsoukos, Study of the electrochemical behaviour of the 7075 aluminum alloy in the presence of sodium oxalate, Corros. Sci. 41 (1999) 941–957. doi:10.1016/S0010-938X(98)00164-4.

[81] M. Amin, M. Saracoglu, N. El-Bagoury, T. Sharshar, M. Ibrahim, J. Wysocka, J. Ryl, Microstructure and Corrosion Behaviour of Carbon Steel and Ferritic and Austenitic Stainless Steels in NaCl Solutions and the Effect of p-Nitrophenyl Phosphate Disodium Salt, Int. J. Electrochem. Sci. 11 (2016) 10029–10052. doi:10.20964/2016.12.17.

[82] M. Giza, P. Thissen, G. Grundmeier, Adsorption Kinetics of Organophosphonic Acids on Plasma-Modified Oxide-Covered Aluminum Surfaces, Langmuir. 24 (2008) 8688–8694. doi:10.1021/la8000619.

[83] E. McCafferty, J.P. Wightman, Determination of the concentration of surface hydroxyl groups on metal oxide films by a quantitative XPS method, Surf. Interface Anal. 26 (1998) 549–564. doi:10.1002/(SICI)1096-9918(199807)26:8<549::AID-SIA396>3.0.CO;2-Q.

[84] Q. Liu, X. Tong, G. Zhou, H2O Dissociation-Induced Aluminum Oxide Growth on Oxidized Al(111) Surfaces, Langmuir. 31 (2015) 13117–13126. doi:10.1021/acs.langmuir.5b02769.

[85] E. Mazzotta, S. Rella, A. Turco, C. Malitesta, XPS in development of chemical sensors, RSC Adv. 5 (2015) 83164–83186. doi:10.1039/C5RA14139G.

[86] E.E. Oguzie, Corrosion inhibition of aluminium in acidic and alkaline media by Sansevieria trifasciata extract, Corros Sci. 49 (2007) 1527–1539. doi:10.1016/j.corsci.2006.08.009.

[87] H. Ashassi-Sorkhabi, Z. Ghasemi, D. Seifzadeh, The inhibition effect of some amino acids towards the corrosion of aluminum in 1M HCl+1M H2SO4 solution, Appl. Surf. Sci. 249 (2005) 408–418. doi:10.1016/j.apsusc.2004.12.016.

[88] S.A. Umoren, E.E. Ebenso, Studies of the anti-corrosive effect of *Raphia hookeri* exudate gum-halide mixtures for aluminium corrosion in acidic medium, Pigment Resin Technol. 37 (2008) 173–182. doi:10.1108/03699420810871020.

[89] I.M. Mejeha, M.C. Nwandu, K.B. Okeoma, L.A. Nnanna, M.A. Chidiebere, F.C. Eze, E.E. Oguzie, Experimental and theoretical assessment of the inhibiting action of Aspilia africana extract on corrosion aluminium alloy AA3003 in hydrochloric acid, J. Mater. Sci. 47 (2012) 2559–2572. doi:10.1007/s10853-011-6079-2.

[90] A. Yurt, B. Duran, H. Dal, An experimental and theoretical investigation on adsorption properties of some diphenolic Schiff bases as corrosion inhibitors at acidic solution/mild steel interface, Arab. J. Chem. 7 (2014) 732–740. doi:10.1016/j.arabjc.2010.12.010.

[91] E.. Ebenso, Synergistic effect of halide ions on the corrosion inhibition of aluminium in H2SO4 using 2-acetylphenothiazine, Mater. Chem. Phys. 79 (2003) 58–70. doi:10.1016/S0254-0584(02)00446-7.

[92] A.M. Abdel-Gaber, B.A. Abd-El-Nabey, I.M. Sidahmed, A.M. El-Zayady, M. Saadawy, Inhibitive action of some plant extracts on the corrosion of steel in acidic media, Corros. Sci. 48 (2006) 2765–2779. doi:10.1016/j.corsci.2005.09.017.

[93] C. Mary Anbarasi, G. Divya, A Green Approach to Corrosion Inhibition of Aluminium in Acid Medium Using Azwain Seed Extract, Mater. Today Proc. 4 (2017) 5190–5200. doi:10.1016/j.matpr.2017.05.026.

[94] J. Fayomi, A.P.I. Popoola, O.S.I. Fayomi, K.O. Babaremu, Data on the effect of temperature variation tendency on the inhibitive absorption of Lasienthera africanum in 0.5M HCl: A necessity, Data Brief. 20 (2018) 2003–2011. doi:10.1016/j.dib.2018.09.019.

[95] J. Ryl, K. Darowicki, P. Slepski, Evaluation of cavitation erosion–corrosion degradation of mild steel by means of dynamic impedance spectroscopy in galvanostatic mode, Corros. Sci. 53 (2011) 1873–1879. doi:10.1016/j.corsci.2011.02.004.

[96] A.A. Khadom, A.S. Yaro, A.A.H. Kadhum, ADSORPTION MECHANISM OF BENZOTRIAZOLE FOR CORROSION INHIBITION OF COPPER-NICKEL ALLOY IN HYDROCHLORIC ACID, J. Chil. Chem. Soc. 55 (2010). doi:10.4067/S0717-97072010000100035.

[97] E.A. Noor, Potential of aqueous extract of Hibiscus sabdariffa leaves for inhibiting the corrosion of aluminum in alkaline solutions, J. Appl. Electrochem. 39 (2009) 1465–1475. doi:10.1007/s10800-009-9826-1.

[98] L.R. Chauhan, G. Gunasekaran, Corrosion inhibition of mild steel by plant extract in dilute HCl medium, Corros. Sci. 49 (2007) 1143–1161. doi:10.1016/j.corsci.2006.08.012.

[99] A.K. Satapathy, G. Gunasekaran, S.C. Sahoo, K. Amit, P.V. Rodrigues, Corrosion inhibition by Justicia gendarussa plant extract in hydrochloric acid solution, Corros. Sci. 51 (2009) 2848–2856. doi:10.1016/j.corsci.2009.08.016.

[100]   I.B. Obot, S.A. Umoren, N.O. Obi-Egbedi, Corrosion inhibition and adsorption behaviour for aluminuim by extract of Aningeria robusta in HCl solution: Synergistic effect of iodide ions, J. Mater. Environ. Sci. 2 (2011) 60–71.

[101]   I.B. Obot, N.O. Obi-Egbedi, S.A. Umoren, The synergistic inhibitive effect and some quantum chemical parameters of 2,3-diaminonaphthalene and iodide ions on the hydrochloric acid corrosion of aluminium, Corros. Sci. 51 (2009) 276–282. doi:10.1016/j.corsci.2008.11.013.

[102]   D.G. Ladha, N.K. Shah, Z. Ghelichkhah, I.B. Obot, F. Khorrami Dehkharghani, J.-Z. Yao, D.D. Macdonald, Experimental and computational evaluation of illicium verum as a novel eco-friendly corrosion inhibitor for aluminium, Mater. Corros. 69 (2018) 125–139. doi:10.1002/maco.201709581.

[103]   M.J. Pellerite, T.D. Dunbar, L.D. Boardman, E.J. Wood, Effects of Fluorination on Self-Assembled Monolayer Formation from Alkanephosphonic Acids on Aluminum: Kinetics and Structure, J. Phys. Chem. B. 107 (2003) 11726–11736. doi:10.1021/jp0354200.

[104]   M. Rbaa, M. Galai, Y. Kacimi, M. Ouakki, R. Touir, B. Lakhrissi, M.E. Touhami, Adsorption Properties and Inhibition of Carbon Steel Corrosion in a Hydrochloric Solution by 2-(4,5-diphenyl-4,5-dihydro-1h-imidazol-2-yl)-5-methoxyphenol:, Port. Electrochimica Acta. 35 (2017) 323–338. doi:10.4152/pea.201706323.

[105]   K. Larouj, K. Ourrak, M. El M'Rabet, H. Zarrok, H. Serrar, M. Boudalia, S. Boukhriss, I. Warad, H. Oudda, R. Touir, Thermodynamic study of corrosion inhibition of carbon steel in acidic solution by new pyrimidothiazine derivative, J. Mater. Environ. Sci. 8 (2017) 3921–3931.

[106]   P. Kwolek, A. Kamiński, K. Dychtoń, M. Drajewicz, J. Sieniawski, The corrosion rate of aluminium in the orthophosphoric acid solutions in the presence of sodium molybdate, Corros. Sci. 106 (2016) 208–216. doi:10.1016/j.corsci.2016.02.005.

[107]   V. Sharma, S. Kumar, S. Bashir, Z. Ghelichkhah, I.B. Obot, A. Kumar, Use of *Sapindus* (reetha) as corrosion inhibitor of aluminium in acidic medium, Mater. Res. Express. 5 (2018) 076510. doi:10.1088/2053-1591/aacf76.

[108]   E.A. Noor, A.H. Al-Moubaraki, Thermodynamic study of metal corrosion and inhibitor adsorption processes in mild steel/1-methyl-4[4'(-X)-styryl pyridinium iodides/hydrochloric acid systems, Mater. Chem. Phys. 110 (2008) 145–154. doi:10.1016/j.matchemphys.2008.01.028.

[109]   I. Ahamad, R. Prasad, M.A. Quraishi, Thermodynamic, electrochemical and quantum chemical investigation of some Schiff bases as corrosion inhibitors for mild steel in hydrochloric acid solutions, Corros. Sci. 52 (2010) 933–942. doi:10.1016/j.corsci.2009.11.016.

[110]   M.M. Solomon, H. Gerengi, S.A. Umoren, Carboxymethyl Cellulose/Silver Nanoparticles Composite: Synthesis, Characterization and Application as a Benign Corrosion Inhibitor for St37 Steel in 15% H_2SO_4 Medium, ACS Appl. Mater. Interfaces. 9 (2017) 6376–6389. doi:10.1021/acsami.6b14153.
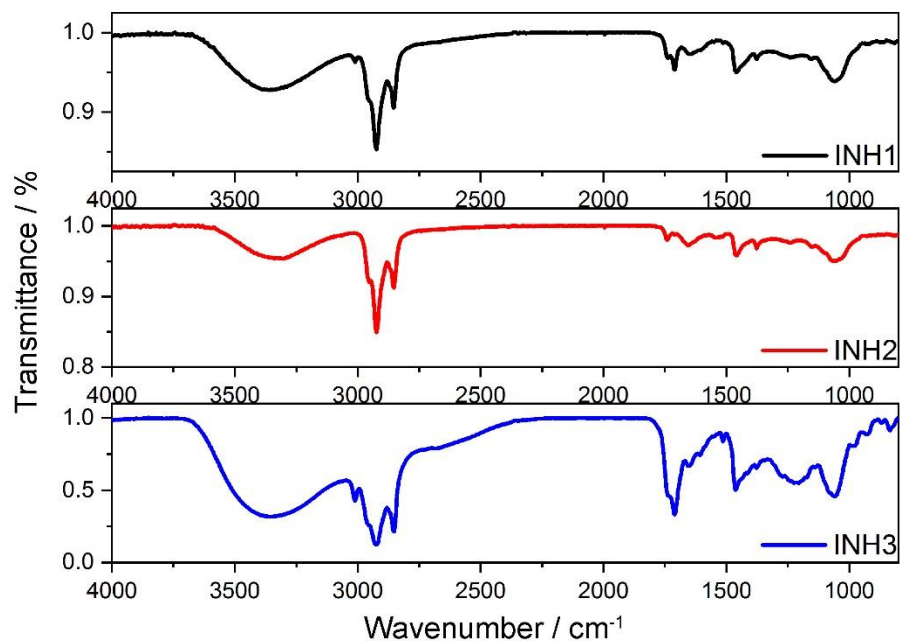
Figure Captions:

Figure 1 - FTIR spectra of the examined bee pollen-based corrosion inhibitor extracts INH1, INH2, INH3.
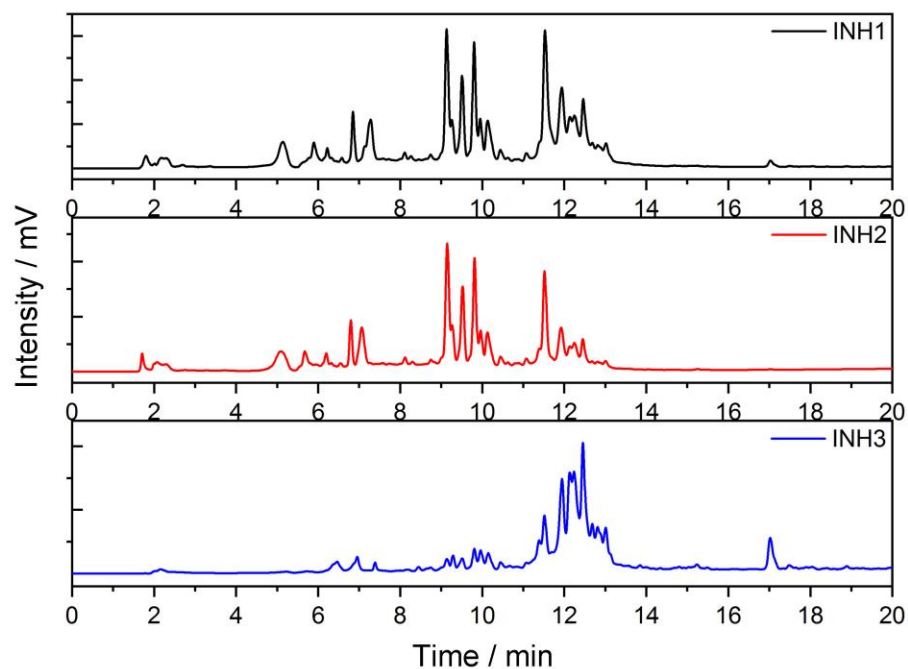

Figure 2 - HPLC chromatograms of the examined bee pollen-based corrosion inhibitor extracts INH1, INH2, INH3.
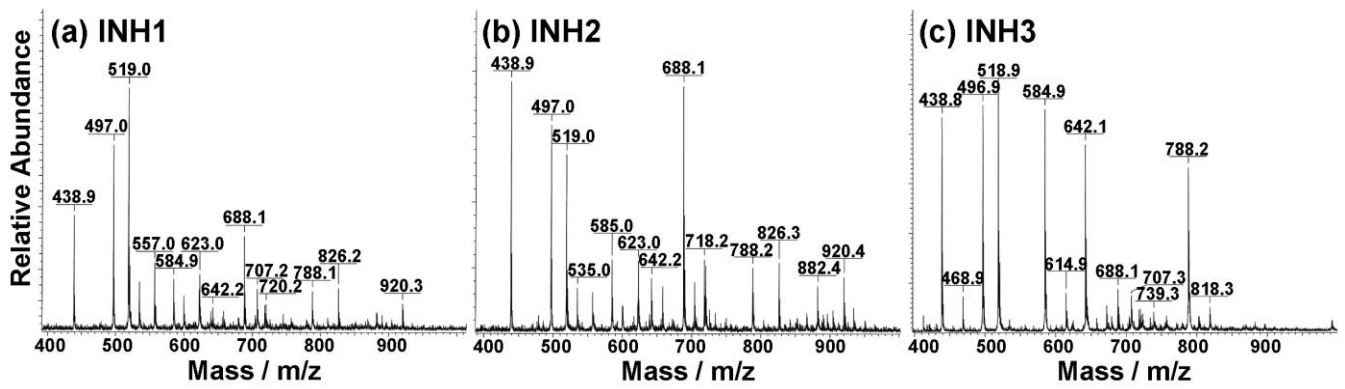
Figure 3 - The MALDI-TOF mass spectra of the of the examined bee pollen-based corrosion inhibitor extracts INH1, INH2, INH3.
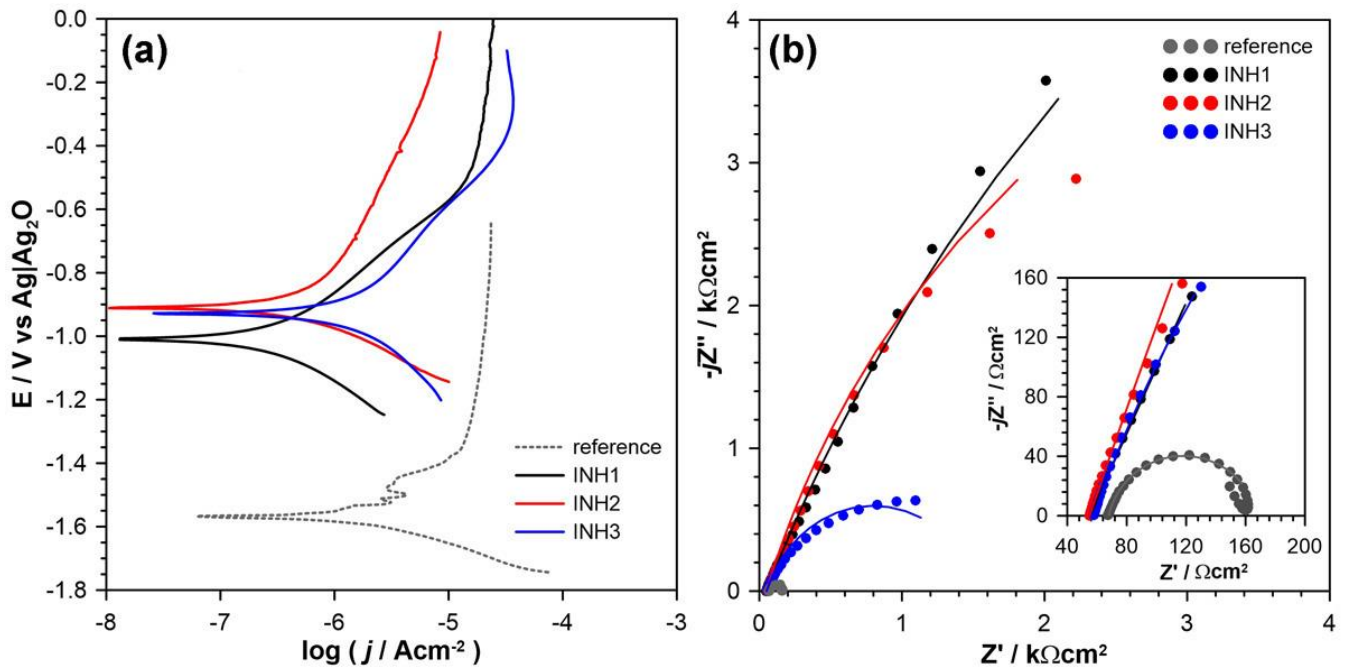

Figure 4 - Corrosion studies of AA5754 in bicarbonate buffer (pH = 11) with and without the bee pollen extracts: (a) potentiodynamic polarization curves, (b) electrochemical impedance spectroscopy, presented as Nyquist plot. On the EIS Nyquist plot, the dots refer to measured impedance while the solid line refer to impedance values calculated with R(QR) EEC.
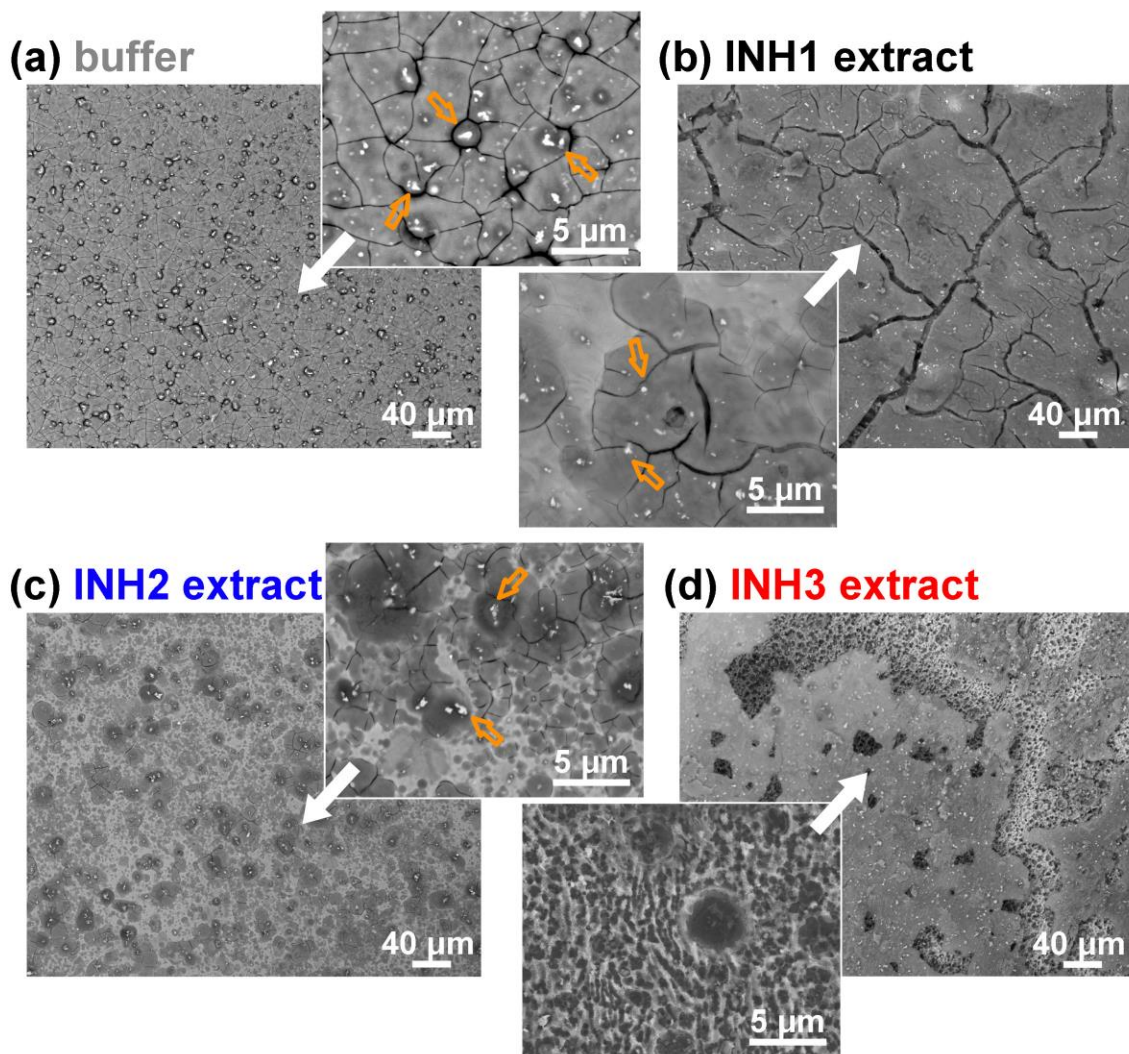
Figure 5 – SEM micrographs of AA5754 in BSE mode recorded after an 18 h exposure to (a) bicarbonate buffer (pH 11), and buffer containing 10 gL^{-1} of studied: (b) INH1, (c) INH2, (d) INH3 bee pollen extracts.
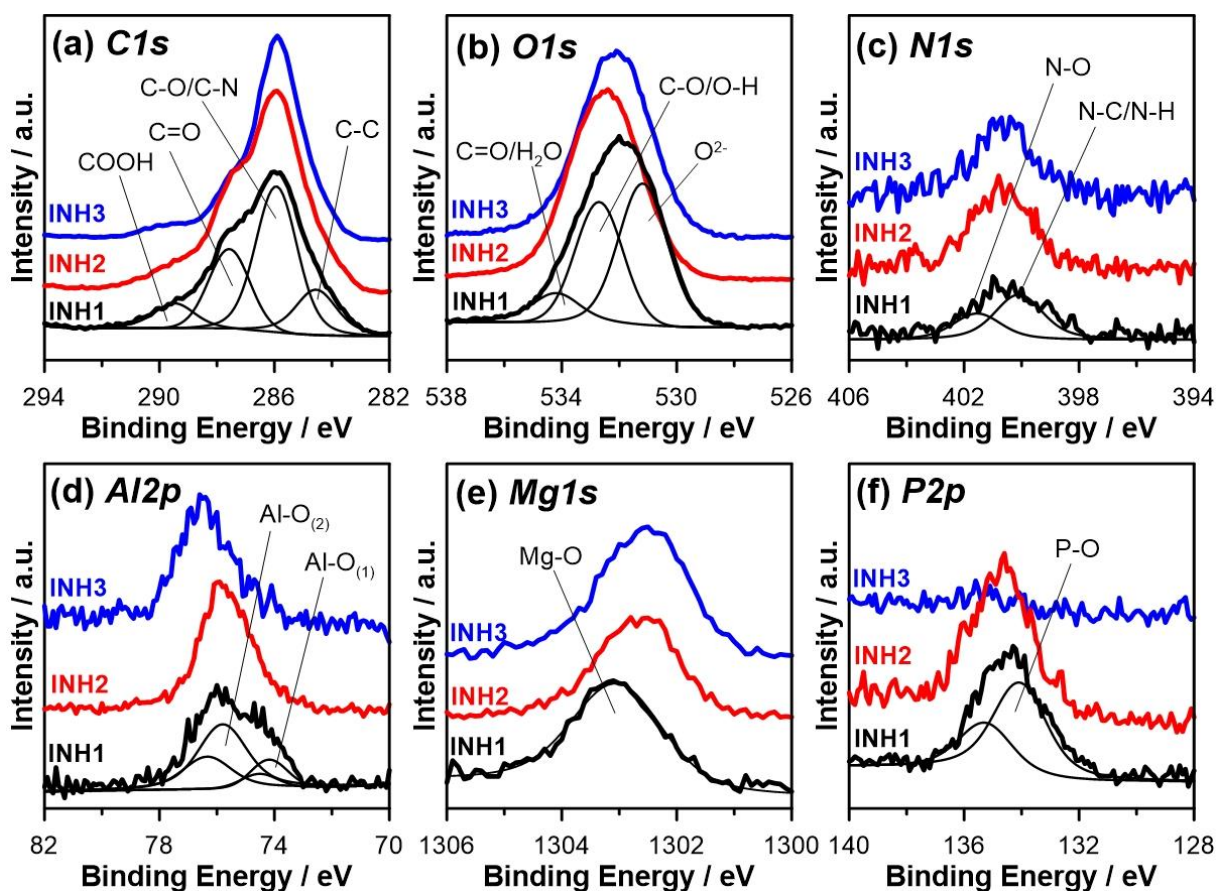
Figure 6 – High-resolution XPS spectra carried out in the (a) *C1s*, (b) *O1s*, (c) *N1s*, (d) *Al2p*, (e) *Mg1s* and (f) *P2p* binding energy range for AA5754 sample exposed to bicarbonate buffer with 10 gL^{-1} addition of INH1, INH2 or INH3 extract.
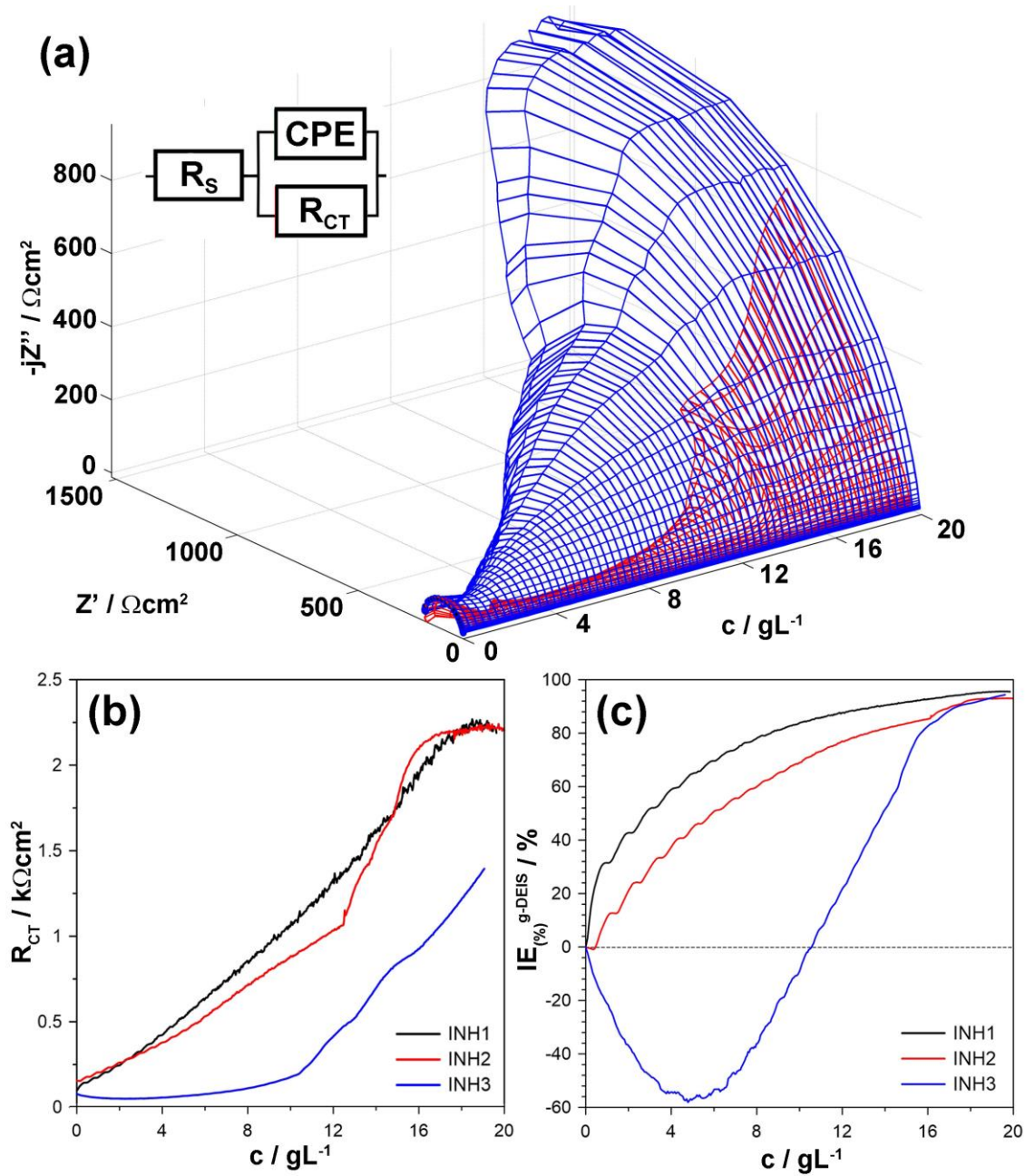
Figure 7 – The results of g-DEIS study: (a) instantaneous impedance spectra in Nyquist plot registered during the injection of INH2 and INH3 extracts; (b) R_{CT} values obtained after R(QR) EEC fitting on the basis of g-DEIS results; (c) changes in inhibition efficiency $IE_\%$/surface coverage θ with inhibitor concentration.
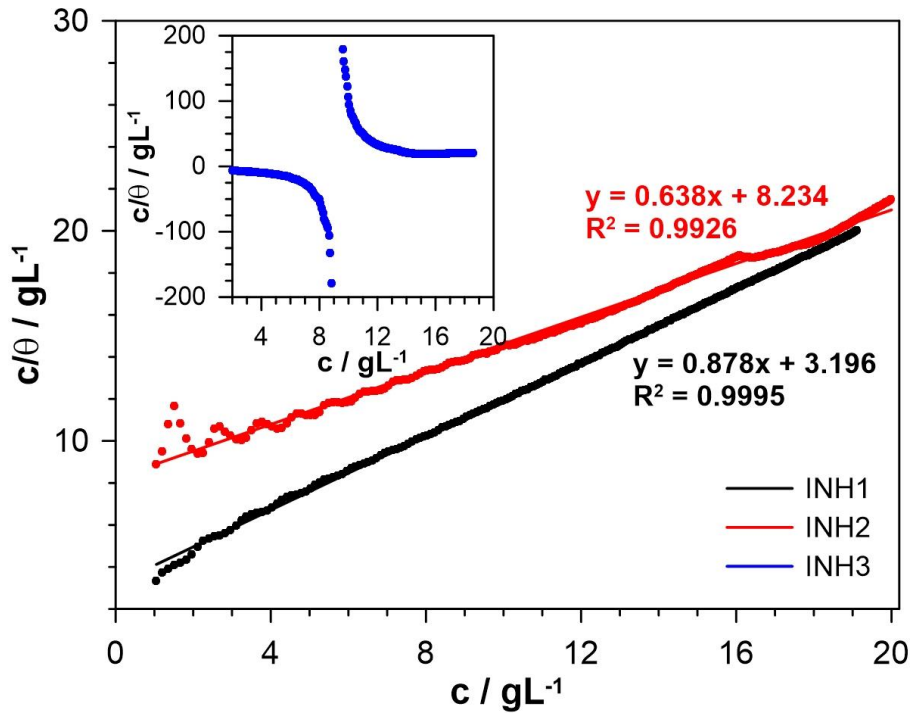
Figure 8 - Langmuir adsorption isotherms drawn with the g-DEIS approach for each studied inhibitor extract.
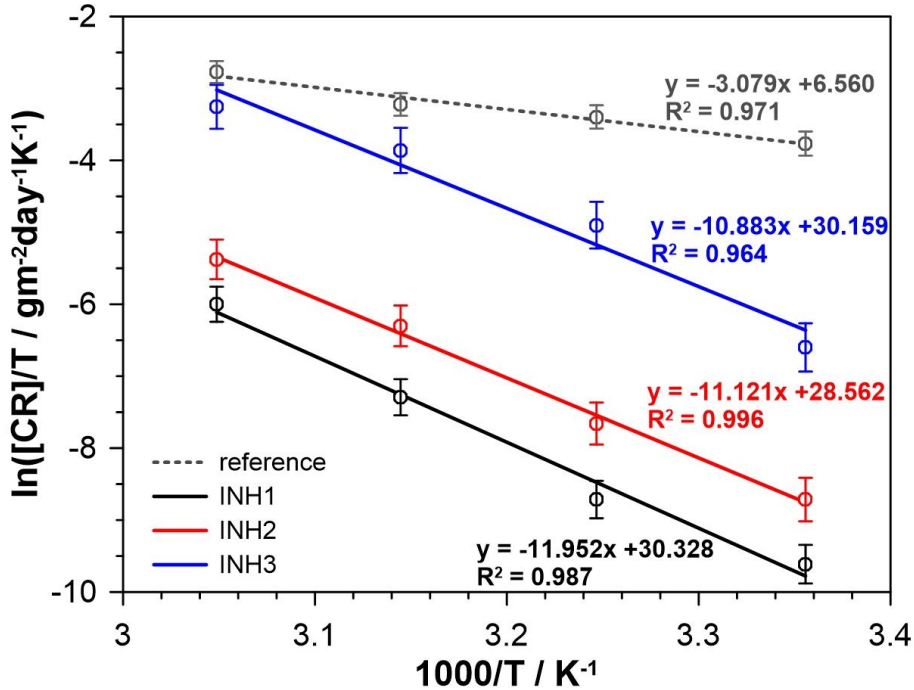

Figure 9 - Transition-state Arrhenius plots for aluminium alloy in bicarbonate buffer (pH = 11) with and without the corrosion inhibitors INH1, INH2, INH3 added at the concentration of 10 gL^{-1}.

Table 1 – The results of corrosion studies and the corrosion inhibition efficiency for AA5754. The calculations were based on the potentiodynamic polarization and EIS data fitted using R(QR) EEC for the bee pollen extract concentration of 10 gL^{-1} in bicarbonate buffer (pH = 11).

	i_{corr} / μAcm^{-2}	$IE_\%^{(pol)}$ / %	R_{CT} / $k\Omega cm^2$	Q / μSs^n	n / -	C_{eff} / μF	$IE_\%^{(EIS)}$ / %
Reference	3.44 ±0.6	--	0.09 ±0.01	41.9 ±0.5	0.89 ±0.02	12.05	--
INH1	0.27 ±0.5	92.2%	15.58 ±0.32	214.7 ±4.1	0.72 ±0.03	8.04	99.7%
INH2	0.41 ±0.7	88.1%	9.26 ±0.26	236.6 ±3.8	0.78 ±0.03	22.45	99.2%
INH3	1.32 ±0.7	61.6%	1.70 ±0.08	157.8 ±3.4	0.77 ±0.03	11.54	94.1%

Table 2 – Percentage contribution (at.%) of various C, O, Al, N, Mg and P chemical states, resulting from high-resolution XPS analysis for AA5754 sample exposed to bicarbonate buffer solution with 10 gL^{-1} of INH1, INH2 or INH3 extract.

	C1s				*O1s*			*Al2p*		*N1s*		*Mg1s*	*P2p*
	C-C	CO/CN	C=O	OC=O	O^{2-}	CO/OH	C=O/H_2O	$AlO_{(1)}$	$AlO_{(2)}$	NO	CN/CH	MgO	P-O
BE/eV	284.6	286.0	287.5	289.4	531.3	532.7	534.2	74.3	76.0	401.7	400.2	1302.7	134.2
INH1	7.8	22.6	12.0	4.4	17.1	17.4	4.4	1.2	4.3	1.5	0.9	2.3	4.1
INH2	8.8	25.7	16.8	3.9	11.5	19.1	4.6	0.2	4.7	0.6	1.0	1.3	1.8
INH3	11.9	44.1	14.6	3.9	9.2	9.0	1.9	--	2.4	0.7	0.7	1.6	--

Table 3 – The values of Gibbs free energy ΔG^* obtained at corrosion inhibitor concentrations 0-20 gL^{-1} and the activation parameters ΔH_a^* and ΔS_a^* for each electrolyte (inhibitor concentration 10 gL^{-1}) in the 25-55 °C temperature range.

	ΔG^* / $kJmol^{-1}$	ΔH_a^* / $kJmol^{-1}$	ΔS_a^* / $Jmol^{-1}K^{-1}$
Reference	--	-7.62	-142.9
INH1	- 5.93	-29.60	54.6
INH2	- 4.66	-27.54	39.9
INH3	--	-26.95	53.2